CCAT mount control using de-convolution for fast scans

Peter M. Thompson[a], Steve Padin[b]
[a]Systems Technology, Inc., Hawthorne, CA, USA, pthompson@systemstech.com
[b]California Institute of Technology, Pasadena, CA USA, spadin@caltech.edu

ABSTRACT

CCAT will be a 25-meter telescope for submillimeter wavelength astronomy located at an altitude of 5600 meters on Cerro Chajnantor in northern Chile. This paper presents an overview of the preliminary mount control design. A finite element model of the structure has been developed and is used to determine the dynamics relevant for mount control. Controller strategies are presented that are designed to meet challenging wind rejection and fast scan requirements. Conventional inner loops are used for encoder-based control. Offset requirements are satisfied using innovative command shaping with feedforward and a two-command path structure. The fast scan requirement is satisfied using a new approach based on a de-convolution filter. The de-convolution filter uses an estimate of the closed loop response obtained from test signals. Wind jitter requirements remain a challenge and additional sensors such as accelerometers and wind pressure sensors may be needed.

Keywords: CCAT, mount control, wind rejection, fast scanning, feedforward, command shaping, de-convolution filter

1. INTRODUCTION

The Cornell Caltech Atacama Telescope (CCAT) project comprises a consortium of Cornell University, California Institute of Technology, University of Colorado at Boulder, University of Cologne, University of Bonn, eight Canadian universities and Associated Universities, Incorporated. For further information about CCAT see Ref. [1]. A view of the structure (from Ref. [2]) is shown in Figure 1. Previous and related work is in Ref. [3, 4, 5, 6, and 7].

A preliminary mount control design for CCAT is presented in this paper. The design uses a finite element model of the structure. The open loop dynamics relevant for mount control are assessed, including the dominant mode shapes and frequencies.

Requirements for the mount control system are presented, and a mount control system for both AZ and EL axes is designed and compared with the requirements. A command-shaping architecture is presented that includes a feedforward network and a two-command path structure. The commands used for fast scans are pre-distorted using a de-convolution filter.

Emphasis is placed on two challenging requirements for wind rejection and fast scans. Meeting the wind rejection requirement is difficult because the structure contains a large amount of carbon fiber, which though very stiff, has a smaller moment of inertia relative to a steel structure, and hence results in higher accelerations for a given wind disturbance force. The scan requirement is based on meeting science objectives that use data collected during fast scans of a region of the sky. Maintaining small following errors over the length of the scan can be accomplished using a

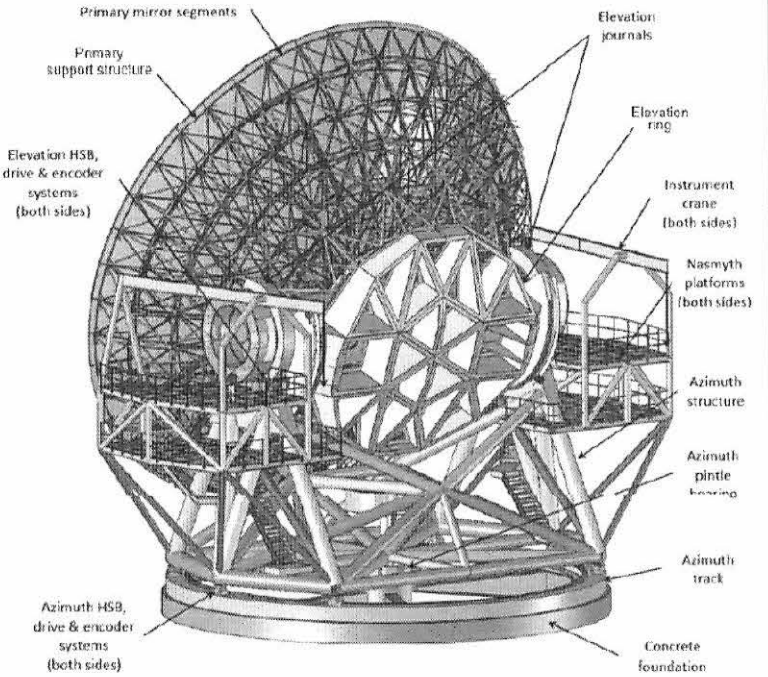

Figure 1: CCAT at 20° elevation, rear isometric view

Ground-based and Airborne Telescopes V, edited by Larry M. Stepp, Roberto Gilmozzi, Helen J. Hall, Proc. of SPIE Vol. 9145, 91451P • © 2014 SPIE
CCC code: 0277-786X/14/$18 • doi: 10.1117/12.2057250

de-convolution filter, which distorts the input AZ and EL scan patterns so that the on-the-sky path meets the requirements.

In the mount control design effort the principle was followed where the controller follows from a good understanding of the "controlled element." This understanding is included in Ref. [3] and is summarized here in Section 2. The wind model assumes fully developed, von Karman turbulence on the M2 and M1 structures. Section 3 describes the wind model. The parameter values are listed in Table 1. The mount control design is presented in Section 4 starting with requirements. The feedback architecture and the various filters are each discussed. Closed loop analysis is presented in Section 5, including stability analysis, nodding performance, and wind jitter.

The requirement for fast scanning over a region of the sky is a performance requirement that distinguishes submillimeter wavelength telescopes from optical telescopes. Section 6 explains why this is hard to do, present a method for meeting the requirement, and then shows by example that the method called "de-convolution" is feasible.

Conclusions of this study and next steps are presented in Section 7.

2. STRUCTURAL MODEL

A finite element model of CCAT was developed by SGH (Ref [2]). The full order model was developed using ANSYS, with different versions of the model available at 90 and 20 degrees elevation. The complete ANSYS model is very important for the mechanical design of the structure, but due to the large size of the model it is inefficient to use for mount control design. For this reason a reduced order model was created that matches the frequency response of the full order model at selected nodes up to 50 Hz. The nodes that are primarily of interest are at the mount control force input locations, encoder locations, and locations on the M1 and M2 structures that can be used to approximate wind disturbance forces. Additional nodes were also selected to provide a good visualization of the low frequency, large spatial resolution structural modes. The model reduction was done within ANSYS, resulting in a model with 674 modes and 54 nodes, with 6 degrees of freedom at each node. The data for this model is stored in a text file that can be loaded into Matlab for analysis and design.

A choice needs to be made on how the include the AZ and EL-axis drives in the reduced order model. The best approach is to release the rotary motion for both drives so that both are free to move. Technically this means there are structural modes at 0 Hz for each drive. If for numerical reasons a structural mode at zero cannot be handled, include a very soft rotary spring on each axis. Just to be clear, do not constrain or include a stiff spring on one axis and free up the other. Free up both axes. Constrain or include a stiff spring if desired *after* creating the reduced order model with both axes free. An advantage of freeing up both axes is the same model can be used for both AZ and EL mount control design.

2.1 EL-Axis Survey

The open loop and locked rotor EL-axis responses are surveyed in Figure 2, where:

- EL is from the motor torque input to the encoder output
- M2 is the response of torque applied at M2 to the angular change at M2
- M1 is tip-Zernike torque applied at M1 to the tip-Zernike angular response at M1

The frequency responses include both the E20 and E90 cases (20 and 90 degrees elevation). The responses are not significantly different; from which it can be inferred that a controller without gain changes can be used over this range of elevation angles. The M1 and M2 responses are locked rotor responses, which are included because they are used to determine the best possible wind rejection. Any response that is "locked" is flat at low frequency, and the resulting steady state compliance is marked on the figures. The locked rotor zeroes for E20 and E90 respectively at 5.79 and 5.96 in the EL responses "flip over" when the EL-axis is locked to become poles at the same frequencies in the M2 response and near-the-same frequencies in the M1 response.

Structural mode shape diagrams at 9.6 and 11.2 Hz are included in Figure 2, which correspond to peaks at (almost) the same frequencies in the EL response. The M1 and M2 structures move differentially at 9.5 Hz and together at 11.1 Hz. The so-called "differential resonance" at 9.5 Hz imposes a limit on performance. This happens indirectly because a structural filter is needed to reduce the gain at the differential resonance, which can only be done by introducing phase lag, which in turn makes it necessary to change the PID gains to introduce more phase lead, which results in lower gain at low frequency, and hence results in lower wind rejection.

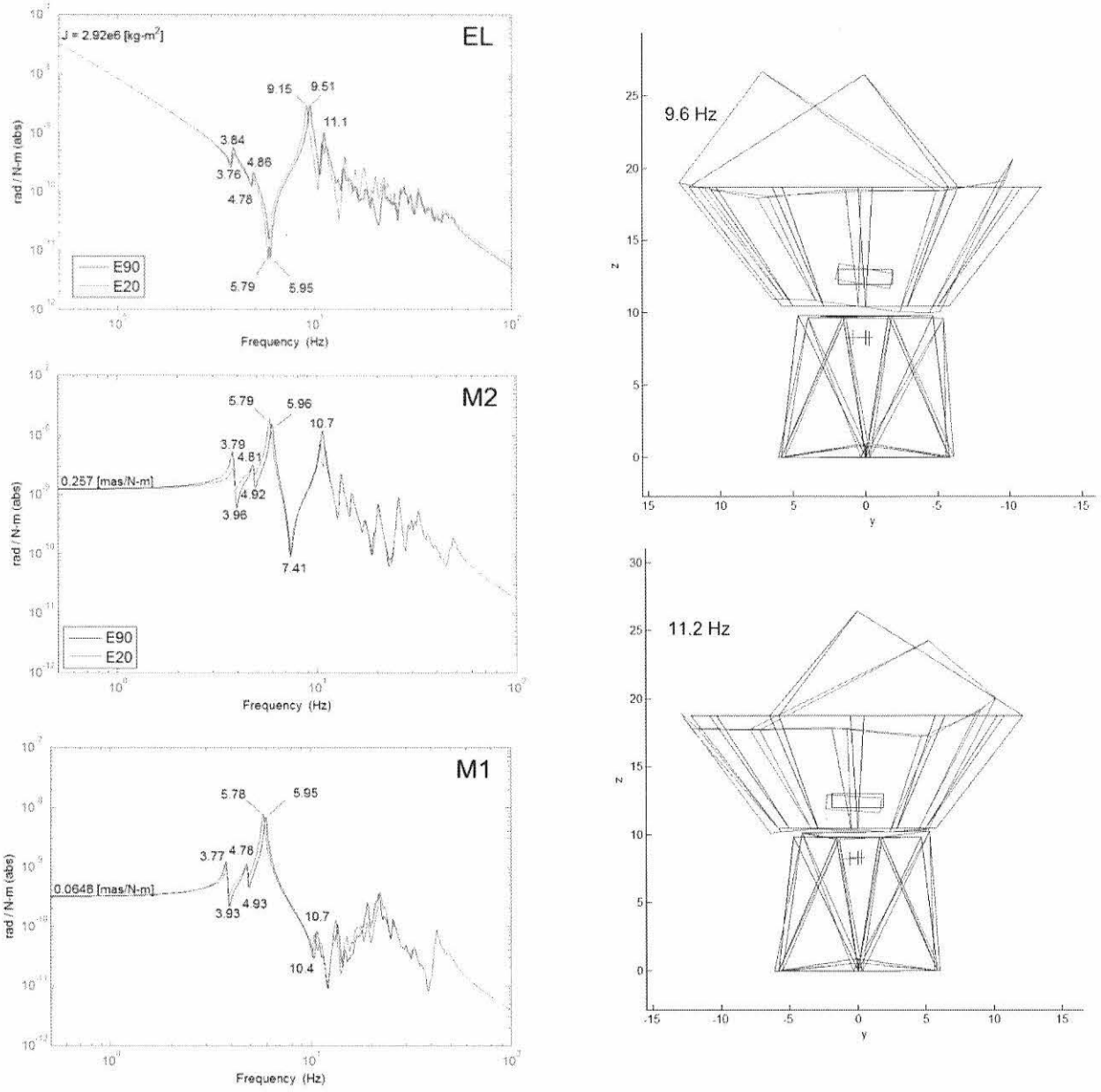

Figure 2: Open loop EL-axis survey

The EL-axis response has a fore-aft-sway mode at 3.84 Hz where the AZ and EL structure move together as a rigid body relative to the pier. The sway mode is almost canceled by the nearby and slightly lower frequency zero at 3.76 Hz, which means this mode can be ignored in the mount control design.

In the mode shape diagrams, the rectangle close to the bottom of the M1 truss represents the EL-axis tube, and the plus at the top of the AZ-structure is the middle location of the EL-axis drive. The lines on the mode shape diagram connect the nodes selected for the reduced order model, and roughly but not exactly correspond to structural members. The "full" mode shape with thousands of lines is available using ANSYS and were used to help understand the structure. The reduced order mode shapes were also used, and arguably are sometimes better at helping to understand relative motion. In any case, to emphasize to design approach actually used, the reduced order mode shape diagrams are included here.

All of the EL-axis responses depend (weakly but a little bit) on whether or not the AZ-axis is closed, and vice-versa. In all of the responses shown in Figure 2 and Figure 3 the drive on the opposite axis is open.

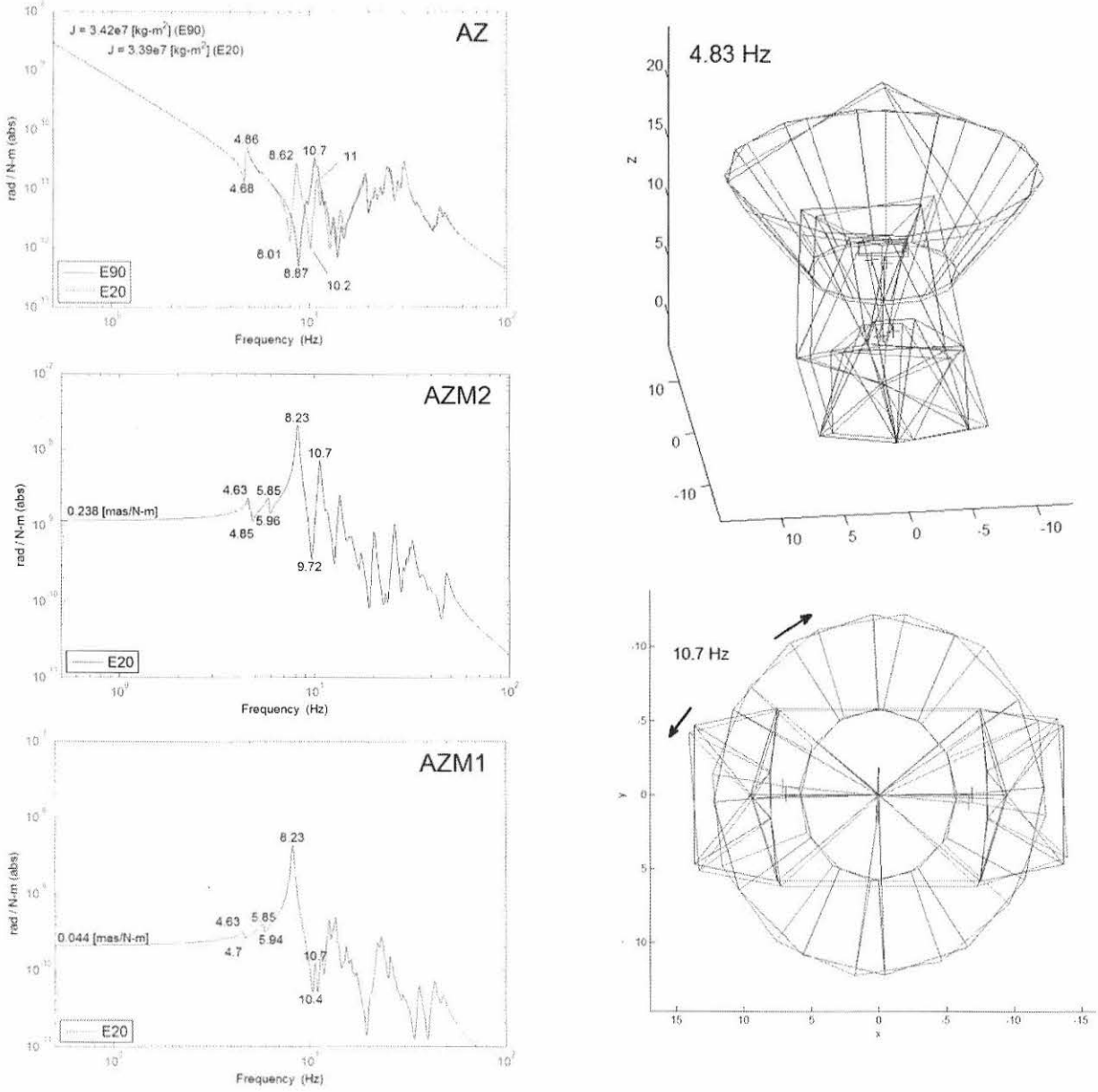

Figure 3: Open loop AZ-axis survey

2.2 AZ-Axis Survey

A similar open loop AZ-axis survey is in Figure 3, where:

- AZ is from the motor torque input to the encoder output
- AZM2 is the response from torque applied at M2 to the angular change at M2 with the AZ-axis locked
- AZM1 is tilt-Zernike torque applied at M1 to the tile-Zernike angular response at M1 with the AZ-axis locked

The moment-of-inertia about the AZ-axis for E20 and E90 changes less than one percent, but there is a significant change in the locked rotor zero (respectively 8.01 to 8.87 Hz) and the differential resonance (respectively 8.62 to 10.7 Hz). The same gains are used in the AZ-axis mount control despite these changes, but a gain schedule will be considered during the detailed design phase. The AZ and EL-structures move together for the mode shape at 4.83 Hz, and differentially for the mode shape at 10.7 Hz. The former is not a factor in the AZ-axis mount control, and the latter limits the AZ-axis bandwidth.

2.3 The Softening Effect of the AZ-Structure

If the EL-structure is mounted on a rigid base and the EL-axis rotor is locked, the dominant frequency of the EL-structure is 10.1 Hz. This is the frequency, and corresponding stiffness, to which the EL-structure was designed. The expectation was the locked rotor zero for the EL-axis drive response would be at 10.1 Hz, or something close. The rigid base locked rotor frequency response at M2 is shown in Figure 4 and should be compared with the M2 response in Figure 2, mounted on the AZ-structure.

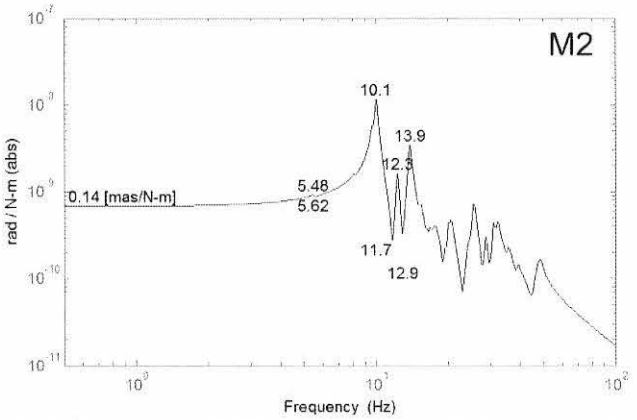

Figure 4: M2 response of EL-structure mounted on a rigid base

The dominant frequency has dropped 41% from 10.1 to 5.96 Hz (at E90), and the rotary compliance at M2 has increased 84% from 0.14 mas/N-m to 0.257 mas/N-m (milli-arc-second per Newton-meter). This is the softening effect of mounting on the AZ-structure. This effect is examined in more detail in Ref [3]. There is no "weak link" in the AZ-structure; the compliance is distributed more-or-less evenly from the hydrostatic bearings at the top of the AZ-structure to the movement of the pier in the ground. This means stiffening any one part of the AZ-structure or pier will not make up the difference. Nevertheless, limited improvements are being considered.

3. WIND MODEL

The distributed wind force on the EL-structure results in torques about both the EL and AZ-axes. The steady state wind force is countered by steady state EL and AZ-axis drive motor torque, which is one part of the calculation for required motor torque. The wind turbulence results in stochastic pointing error. The wind turbulence is approximated using a von Karman spectrum, injected into the system as four different disturbance inputs: M1 and M2, AZ and EL. The parameter estimates for the von Karman spectrum are listed in Table 1.

3.1 Disturbance inputs

Define an EL-structure Cartesian coordinate system where the EL-axis rotates about the x-axis, the z-axis is positive up, and the y-axis is the right-hand complement.

M2 EL-Axis: The wind is a point force in the y-axis direction, perpendicular to the EL-axis of rotation, with an rms value of F, applied at a single node on the M2 structure a distance R_{M2} from the EL-axis of rotation. The resulting torque about the EL-axis is $T_{ELM2} = FR_{M2}$.

M2 AZ-Axis: The wind is a point force in the x-axis direction, perpendicular to the AZ-axis of rotation, with an rms value of F, applied at the same node on the M2 structure, with a lever arm of $R_{M2}\cos(EL)$. The resulting torque about the AZ-axis is $T_{AZM2} = FR_{M2}\cos(EL)$. When the telescope is pointing at Zenith the elevation angle is EL=90 deg and there is no wind torque about the AZ-axis.

M1 EL-Axis: The total wind force in the z-axis direction is assumed to be uniformly distributed on one-half of M1, divided in half by the y-axis, resulting in a torque about the EL-axis. Call this the tip direction. This is equivalent to assuming half of the force is in opposite directions on either side of M1. The torque about the EL-axis is $T_{ELM1} = \int_A y dF = FR_{eff}$, where the effective radius of M1 works out to be $R_{eff} = (4/(3\pi))R_{M1} \approx 0.424R_{M1}$ and where R_{M1} is the actual radius of M1. In the reduced order finite element model, the total force is distributed about the available nodes on the M1 structure as described in Ref. [3].

M1 AZ-Axis: In a similar way the total wind force in the z-axis direction is assumed to be uniformly distributed on one-half of M1 as divided by the x-axis. Call this the tilt direction. The resulting torque about the AZ-axis is $T_{AZM1} = \cos(EL)FR_{eff}$.

3.2 von Karman Spectrum

The wind force on a structure due to turbulence is assumed to satisfy the following von Karman spectra:

$$\Phi(f) = F^2 \frac{(0.77/f_0)}{[1+(f/f_0)^2]^{7/6}}$$

Where the rms wind force is:

$$F = \tfrac{1}{2}\rho U^2 C_D A d$$

The external wind speed of U_∞ is decreased to $U = \mu U_\infty$ at the M2 and M1 structures. The parameter ρ is the density of air, C_D is the drag coefficient, A is the area of the structure, and d is a de-correlation coefficient. The von Karman break frequency is $f_0 = U/D$ where D is the characteristic length of the turbulence, equal to the dome opening. The von Karman parameters used for the M2 and M1 structures are listed in Table 1. The turbulence model is assumed to be the same in each of the x, y, and z directions.

Table 1: Wind Model Parameters

Parameter	Definition	M2	M1
Independent parameters			
U_∞ [m/sec]	90th percentile external wind speed	9	9
μ [unitless]	Wind speed reduction factor	0.4	0.2
ρ [kg/m^3]	Density of air	0.7	0.7
C_D [unitless]	Drag coefficient	1	1
D [m]	Characteristic length (equal to dome opening)	30	30
d [unitless]	Decorrelation factor	1 (worst case)	1 (worst case)
A [m^2]	Area of the structure	9	245 (1/2 of M1)
Calculated parameters			
U [m/sec]	90th percentile wind speed at the structure	3.6	1.8
F [N]	rms force	40.8	278
f_0 [Hz]	von Karman break frequency	0.12	0.06

3.3 Decorrelation

M2 Structure: Decorrelation occurs due to vortex shedding that changes the von Karman spectrum so there is more energy at high frequency. This shift tends to reduce the rms response and is included in the model by using a decorrelation factor $d < 1$. This effect is considered small (perhaps 10%) and the worst case value $d = 1$ is used for M2 wind analysis.

M1 Structure: The worst case decorrelation of $d = 1$ assumes all of the available force is applied in either the tip or tilt direction. In reality only a portion is applied in tip and tilt. Some of the force, for example, is uniform across M1, which does not result in torque about either axis. A reasonable assumption for the distribution of the total force is divide the variance among Zernikes, with ¼ of the variance in the piston direction, ¼ in the tip direction, ¼ in the tilt direction, and the remaining ¼ distributed among the higher order Zernikes [Ref 8]. The decorrelation coefficient is applied to the rms force, and so would be $d = \text{sqrt}(¼) = ½$ in each of the tip and tilt directions. In this way the wind force and hence the torque on M1 can be reduced from the worst case assumption of $d = 1$.

4. MOUNT CONTROL DESIGN

4.1 Requirements

Performance requirements based on science objectives flow down to the following set of qualitative and quantitative requirements used for the control system design:

- Maximize wind rejection (by maximizing low-frequency loop gain)
- Acceptable robustness (phase margin > 30 deg, gain margin > 6 dB)
- Structural peaks gain stabilized (peaks magnitudes –6 dB)
- Use feedforward to improve nodding performance
- Shape the pointing commands with velocity and acceleration limits

Drive parameters are listed in Table 2 (Table I from Ref. [4]). Numerical requirements for nodding, wind jitter and scanning are introduced in the sections where the results of the preliminary design are analyzed.

4.2 Feedback Architecture

The mount control architecture in Figure 5 was used for the preliminary design. The only sensors are the encoders. The heart of the controller in Figure 5a is a Proportional-Integral-Derivative (PID) compensator with a structural filter. The diagram shows disturbance inputs for wind, torque ripple, and encoder quantization. The axis rotations at the M1 and M2 locations are used to estimate wind jitter and scanning performance. These rotations are similar to (but not quite the same as) line-of-sight variations computed using ray-tracing on distorted structures.

A choice needs to be made to use just position feedback or both velocity and position. The velocity is derived from the same encoder. Separate velocity and position loops are shown in Figure 5b and is the preferred architecture going forward. Both architectures are the same in regards to the disturbance responses, but the command response differs. The two loop structure is preferred because it provides more lag in the command path and hence results in less structural vibration, and because it results in a feedforward design that is less sensitive to parameter changes in the structure.

Both one and two path versions of the command shaper are shown respectively in Figure 5b and c. The one-path version is the usual approach. Offsets are on-the-sky and injected before the pointing model. The two-path version preserves the on-the-sky offsets with improved transient response. The commands from the pointing model pass through one or two minimum time command shapers which limit both the velocity and acceleration. The velocity limit is based on available braking and the acceleration limit on the available power. The command shaper has worked successfully on Keck and is recommended for use on CCAT. The shaped command is passed through high order low pass filter that limits the jerk. The feedforward network, which must be properly tuned, results in small moves with less overshoot and faster settling. Further details on the two-path version are in Ref. [7].

4.3 PID Design

The three gains of the PID controller are computed as functions of three design parameters. The design parameters are exactly achieved for a rigid body system, and close enough otherwise. The design parameters are:

f_c [Hz] = unit magnitude crossover frequency
PM [deg] = phase margin
LGM [dB] = lower gain margin

The phase margin is extra phase lag that destabilizes the system, and the lower gain margin is the gain reduction that destabilizes the system. It follows non-obviously that:

$$\begin{aligned} k_i &= -\beta\omega_c^2 / (\text{lgm} \times \text{sqrt}(1+\beta^2)) \\ k_p &= \beta(k_i - \omega_c^2)/\omega_c \\ k_r &= \text{lgm} \times J \times k_i / k_p \end{aligned} \quad \text{where} \begin{cases} \beta = \tan(90 + \text{PM}) \\ \text{lgm} = 10^{\text{LGM}/20} \\ \omega_c = 2\pi f_c \end{cases} \tag{1}$$

The rate gain varies with the moment of inertia J and hence is a very large number. The other gains end up being modest sized numbers. This method is from Ref. [6]. Disturbance rejection is increased by increasing f_c, decreasing PM and decreasing LGM. Robustness is increased by going the other way. The goal is to move f_c closer of the locked rotor zero. Within 50% would be very good, and about 40% is achieved.

Table 2: Drive Parameters

Parameter	AZ	EL
Scan speed	$\frac{1}{3}^{\circ}\mathrm{s}^{-1} \times \lambda/350\ \mu\mathrm{m}$	$\frac{1}{6}^{\circ}\mathrm{s}^{-1} \times \lambda/350\ \mu\mathrm{m}$
Scan acceleration	$\frac{1}{3}^{\circ}\mathrm{s}^{-2} \times \lambda/350\ \mu\mathrm{m}$	$\frac{1}{3}^{\circ}\mathrm{s}^{-2} \times \lambda/350\ \mu\mathrm{m}$
Slew speed	$3^{\circ}\mathrm{s}^{-1}$	$3^{\circ}\mathrm{s}^{-1}$
Slew acceleration	$2^{\circ}\mathrm{s}^{-2}$	$2^{\circ}\mathrm{s}^{-2}$
Axis inertia	2.6×10^{7} kg m^2	2.6×10^{6} kg m^2
Motor radius	9.5 m	4 m
Torque for slew acceleration	9.1×10^{5} Nm	9.1×10^{4} Nm
Available motor torque	1.1×10^{6} Nm	1.8×10^{5} Nm

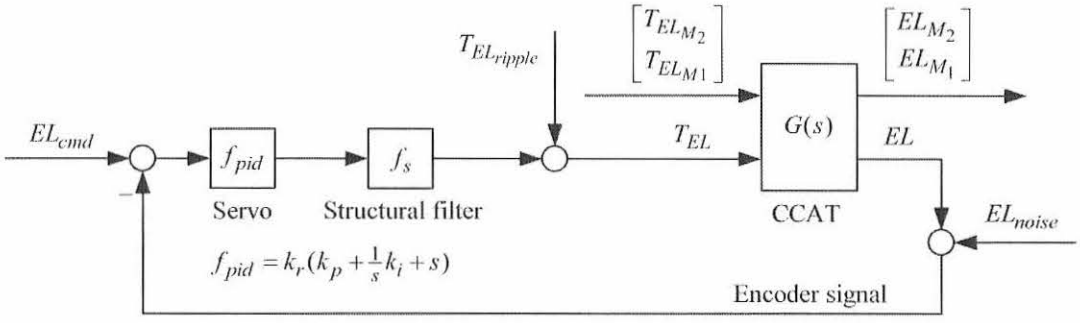

a) PID and structural filter (shown for EL-axis, similar for AZ-axis)

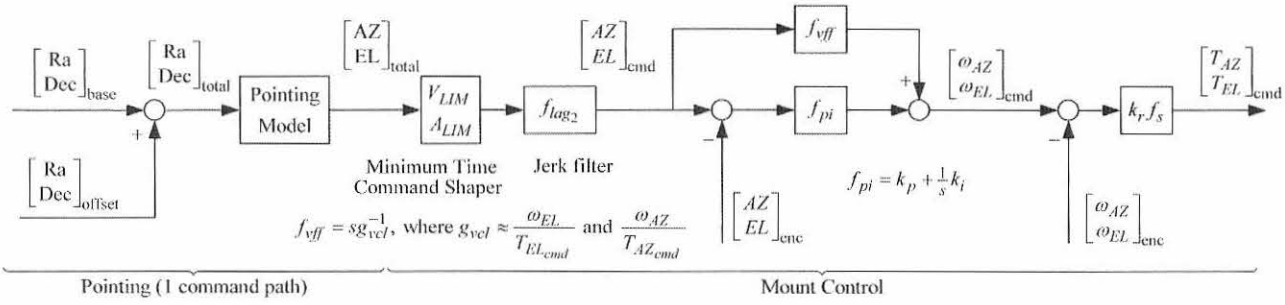

b) Pointing, command shaping, and feedfoward (1 path)

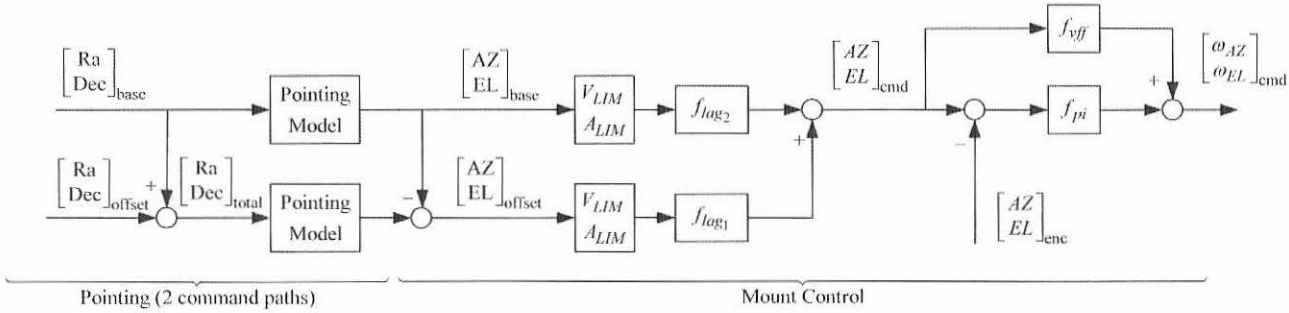

c) 2 path version

Figure 5: Mount control feedback architecture

4.4 Structural Filter Design

The structural filter gain stabilizes the structural modes by reducing all of the peaks to −6 dB or lower. The filter is a series of lags and/or notches with a dc gain of one. There is a difficult tradeoff in the structural filter design between a potentially large amount gain reduction (for gain stability) and a small amount of phase lag (for better performance). The following filter called a "staggered notch" worked well for the preliminary design:

$$f(s) = \frac{(s/\omega_n)^2 + 2\zeta_n(s/\omega_n) + 1}{(s/\omega_d)^2 + 2\zeta_d(s/\omega_d) + 1}$$

Place the pole frequency at ω_d rad/sec near the locked rotor zero and the zero at ω_n near the differential resonance. This "stagger" in frequencies results in significant gain reduction. Further reduce the gain at the differential resonance by setting the numerator damping ratio ζ_n to 0.2 or lower. Values less than about 0.05 are not desired because the design becomes sensitive to the exact location of the differential resonance. The denominator damping ratio of $\zeta_d = 0.5$ provides a good balance with low phase lag without a significant change in gain near the locked rotor zero. Further lags at higher frequency are good design practice. Adjustments in the structural filter will likely be needed as the model matures and then again when the response of the actual structure is measured. The goal is to use one set of constant parameters for each axis, each set of parameters good for all elevation angles.

4.5 Feedforward Design

The feedforward network inverts the closed velocity loop response and ideally is a pure velocity feedforward, which in Laplace notation is $f(s) = s$. In practice the velocity loop has lag which must also be inverted using lead, and a filter is recommended of the form $f(s) = s(as^2 + bs + 1)$. The parameters of the feedforward network can be estimated from the finite element model and eventually from measurements. The feedforward filter is implemented in combination with the jerk filter. The jerk filter must be higher than third order to prevent the implementation of potentially noisy derivatives. The details are in Ref. [3]. Tuning is important. Stability is not a problem, but mismatches result in overshoot, the reduction of which is the goal.

4.6 Jerk Filter Design

Step changes in acceleration are prevented using a linear time invariant filter called a jerk filter. For the one-path command shaper the jerk filter must have zero velocity error (called f_{lag2}). Technically, $(f_{lag2} - 1)/s = 0$ as $s \to 0$. For the two-path solution, better offset performance is obtained by passing the offset portion through a zero position error filter (called f_{lag1}). Sixth order filters were used as shown below:

$$f_{lag_1}(s) = \frac{1}{(\tau_{fast}s + 1)^6}, \quad f_{lag_2}(s) = \frac{(\tau_{slow} + 5\tau_{fast})s + 1}{(\tau_{slow}s + 1)(\tau_{fast}s + 1)^5}$$

Time constants using in the preliminary design are $1/(2\pi\tau_{fast}) = 8$ Hz and $1/(2\pi\tau_{slow}) = 0.33$ Hz.

5. MOUNT CONTROL ANALYSIS

5.1 Stability Analysis

The controller gains are not included here but the resulting loop transfer functions are shown in Figure 6. The "loop transfer function" is the frequency response of the open loop system response times the controller filters. This is the response that is shaped by the controller design. The design objectives are to maximize both the crossover frequency fc and the low frequency gain, with the limitation of keeping the structural peaks all below −6 dB. The achieved crossover frequencies for the EL and AZ-axes are respectively 2.5 and 2.9 Hz, respectively 40% and 36% of the locked rotor zeroes at 6 and 8 Hz. The highest structural peak is about −5 dB. The phase margins (PM) are well above 30 degrees. The delay margins (DM) are noted in the figure and are the added delay that destabilizes. In both loops the sway mode is "phase stabilized," which means the phase blips due to these modes increase and hence are not a stability problem. The design is considered aggressive, which can be made even more so by lowering the phase margin.

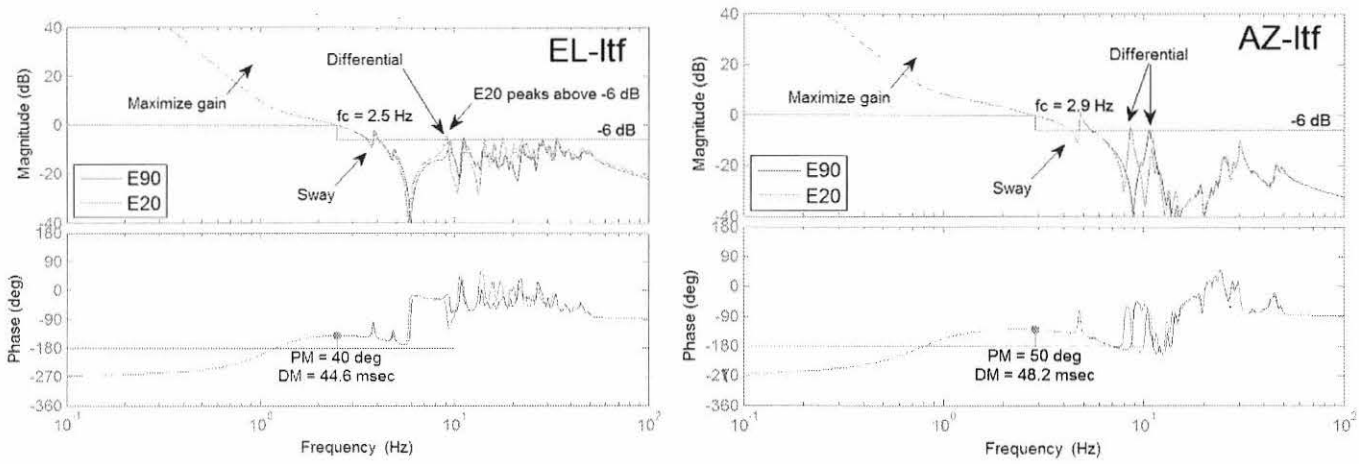

Figure 6: Stability Analysis

5.2 Nodding Analysis

The requirement for a one degree nod is to settle within one-tenth beam in 3 seconds. For beamwidths of λ = 1000 and 350 microns this translates to settling error less than $\lambda/1000$ = 1.00 and 0.35 ArcSec. The two-path command shaper in Figure 5c is needed to meet the 3 second requirement. A plot of the simulation results is not included here, but the achieved settling times are listed below:

```
Error < 1.00 ArcSec, EL = 1.72 [sec], AZ=2.22 [sec]
Error < 0.35 ArcSec, EL = 2.52 [sec], AZ=2.78 [sec]
```

For smaller moves the nodding requirement is stated using number of beamwidths, with the settling time being the time for the response to stay within 1/10th beamwidth. The 350 micron results are reported here. Simulation results are plotted in Figure 7 for nods of 3, 5, 10, and 20 beamwidths. The settling times are listed below:

```
ytarget=  3 [beamwidths] (10.5 [ArcSec]), EL = 1.23 [sec], AZ=1.21 [sec]
ytarget=  5 [beamwidths] (17.5 [ArcSec]), EL = 1.52 [sec], AZ=1.45 [sec]
ytarget= 10 [beamwidths] (35.0 [ArcSec]), EL = 1.81 [sec], AZ=1.72 [sec]
ytarget= 20 [beamwidths] (70.0 [ArcSec]), EL = 2.12 [sec], AZ=2.10 [sec]
```

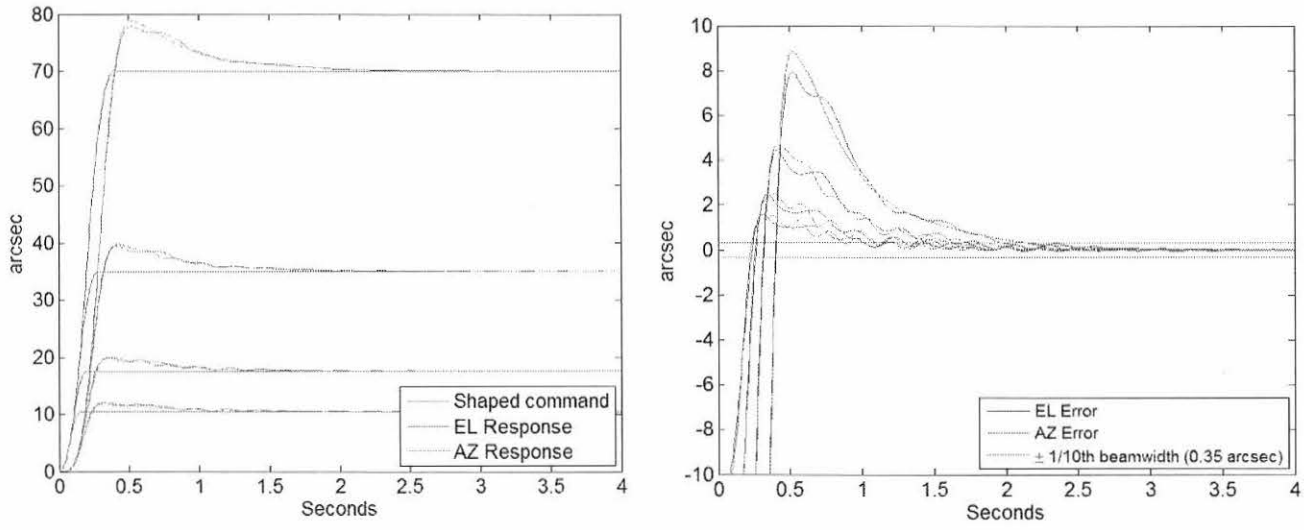

Figure 7: Nodding Analysis (350 micron bandwidth)

5.3 Wind Jitter

The requirement for on-sky wind jitter is less than 0.2 ArcSec rms for 90th percentile external wind speed. The locked rotor M2 and M1 wind response transfer functions determine the ideal wind rejection using encoder-based control. The ideal and achieved versions are compared in Table 3. The "hump" near 1 Hz is the extra response due to mount control. The hump is reduced as the mount control bandwidth increases. The moment-of-inertia is also important, and the large size of the hump in the EL-axis responses is in part a consequence of using a carbon fiber truss rather than a steel truss.

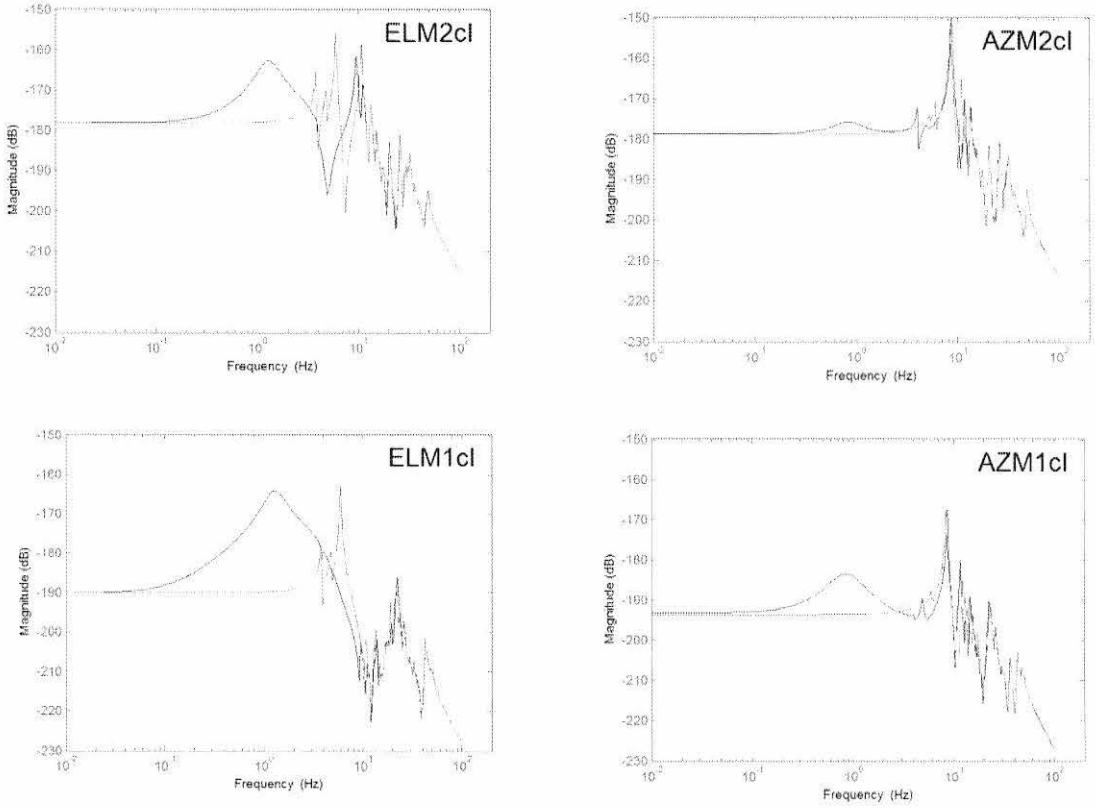

Figure 8: Wind Response Analysis

Numerical results are given in Table 3 for the worst case with no decorrelation, and then using a reasonable estimate of decorrelation. Just the on-sky results are given here. The EL-axis rms contributions from M1 and M2 are about equal, and the total rms for the EL-axis is about twice the total contribution of the AZ-axis. It is seen that the on-the-sky results do not meet the requirements. Neither do the ideal, locked-rotor results, which means that no encoder-based mount control system can meet the wind jitter requirement with the current structure. Either the structure needs to be stiffened, or the mount control needs to be changed to include sensors that somehow measure M2 movement.

Table 3: Wind Jitter Performance Results

	Ideal (ArcSec rms)	Achieved (ArcSec rms)
On-sky rms, axes added in quadrature, no decorrelation		
E90	0.242	0.415
E20	0.302	0.470
On-sky rms, axes added in quadrature, d=0.5 for M1 tip and tilt		
E90	0.195	0.296
E20	0.251	0.345

6. FAST SCAN PERFORMANCE

An important requirement is to scan a region of the sky uniformly to minimize image artifacts. CCAT will use Lissajous patterns, and similar continuous scans, with no blanking during turn-arounds. Simple versions of the Lissajous scan patterns were used for the preliminary design, with the maximum velocity and acceleration of the scan equal to the maximum available velocity and acceleration. The error used to assure no missed segments during the scan is one-half beamwidth, which is $\lambda/200 = 1.75$ ArcSec for a $\lambda = 350$ micron beamwidth.

To start the analysis, consider a sinusoidal scan in just one axis, with simulation results shown in Figure 9. It is seen that the error far exceeds 1.75 ArcSec. Why did this happen? Mount control systems are designed for zero position error for constant velocity inputs. Standard mount control systems work for raster scans because each scan line is (not quite but very nearly) a constant velocity input. The sinusoidal input, and more generally Lissajous scan patterns, are nowhere close to being constant velocity.

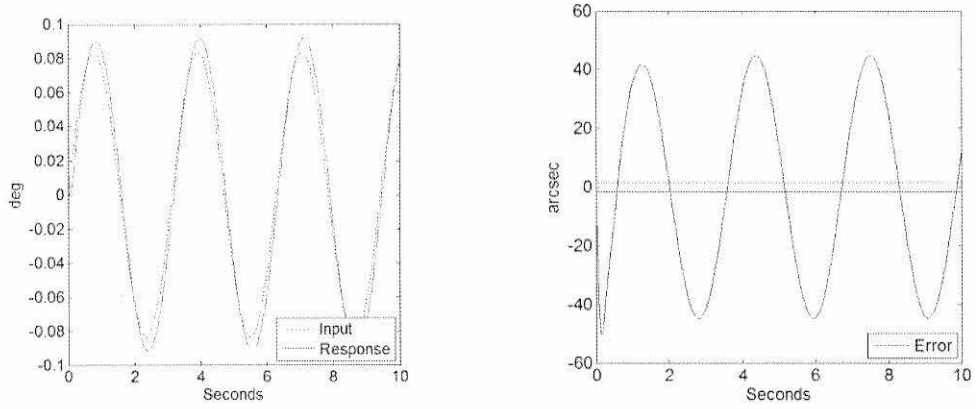

a) Response b) Error

Figure 9: Sinusoidal scan in one axis

The proposed approach is to pre-distort the scan commands so that the achieved on-the-sky pattern is the desired pattern. This method is demonstrated for sinusoidal inputs in Figure 10. The response of a linear system to input $u(t) = A\sin(\omega t)$ is $y(t) = AR\sin(\omega t + \phi)$, where $g(j\omega) = R\exp(j\phi)$ is the response of the system at the input frequency. Use the pre-distorted input $\hat{u}(t) = (A/R)\sin(\omega t - \phi)$. The Lissajous pattern in Figure 10a is a sinusoid in each axis. The error response in Figure 10b is without pre-distortion and in Figure 10c after pre-distortion. It takes about 3 seconds for the error to settle, but then settles to well less than the required value of 1.75 ArcSec.

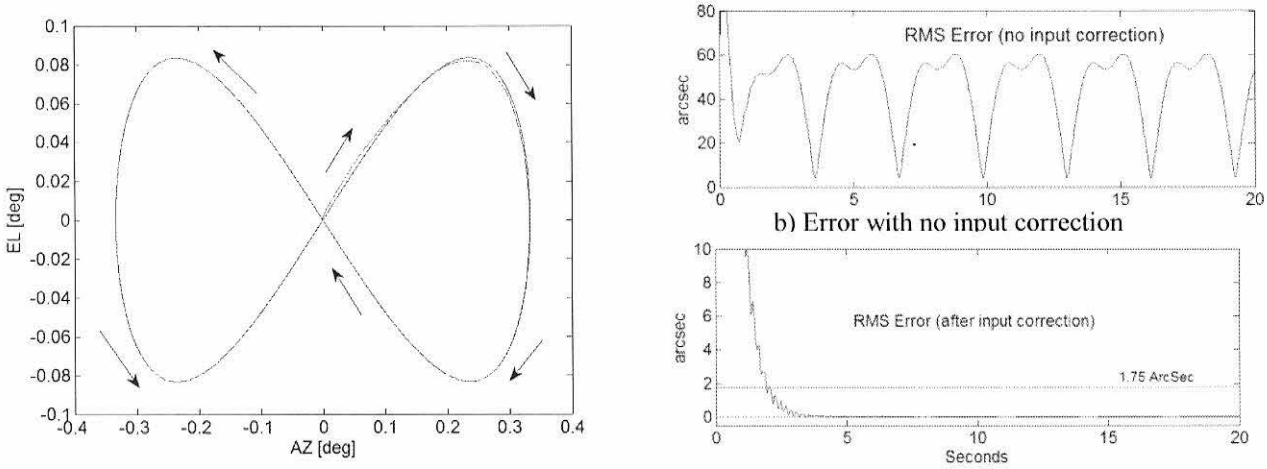

a) Response b) Error with no input correction b) Error after input correction

Figure 10: 350 micron Lissajous Scan

The gain of the system at the input frequency needs to be known to a high degree of accuracy. Define R as the assumed gain and define $R + \varepsilon$ as the actual gain. Using trigonometric identities, it works out that the steady state error will be less than the required value of E if the gain error is $\varepsilon < E/A$. In the Figure 10 example, E = 1.75 ArcSec, A = 300 ArcSec, and the gain error works out to be less than about 1/2 percent.

The pre-distortion scheme used in Figure 10 shows promise but is not sufficient. Constant gain sinusoids, or more generally a constant gain Fourier series, is not sufficient for a region-filling Lissajous pattern. There are two problems with the example in Figure 10, the settling time is too long and more importantly, the gain of the input signal cannot be constant. A pre-distortion scheme based on the steady state frequency response is therefore not sufficient.

The recommended approach is called "de-convolution." Define $u(t)$ as the desired axis command, $g(t)$ as the impulse response of the closed loop system, and then the encoder response $y(t)$ is the convolution:

$$y(t) = \int_{t_0}^{t} g(\tau)u(t-\tau)d\tau$$

The sampled version of the convolution can be written as the matrix product $y = Ug$, where U is a matrix with the samples of u along diagonals and sub-diagonals. The impulse response is estimated using de-convolution:

$$\hat{g} = U^{+}y$$

Where U^{+} is the pseudo-inverse. The estimated impulse response is used to build another banded matrix $\hat{G}$. The distorted input that achieves $y = u$ is computed using a second de-convolution:

$$\hat{u} = \hat{G}^{+}u$$

So there are actually two de-convolutions, one to estimate the impulse response, and a second to create the distorted input. A nice feature of working with impulse responses is number of degrees of freedom does not need to be known. The de-convolution method is demonstrated in Figure 11. The example uses a structure with 676 dof.

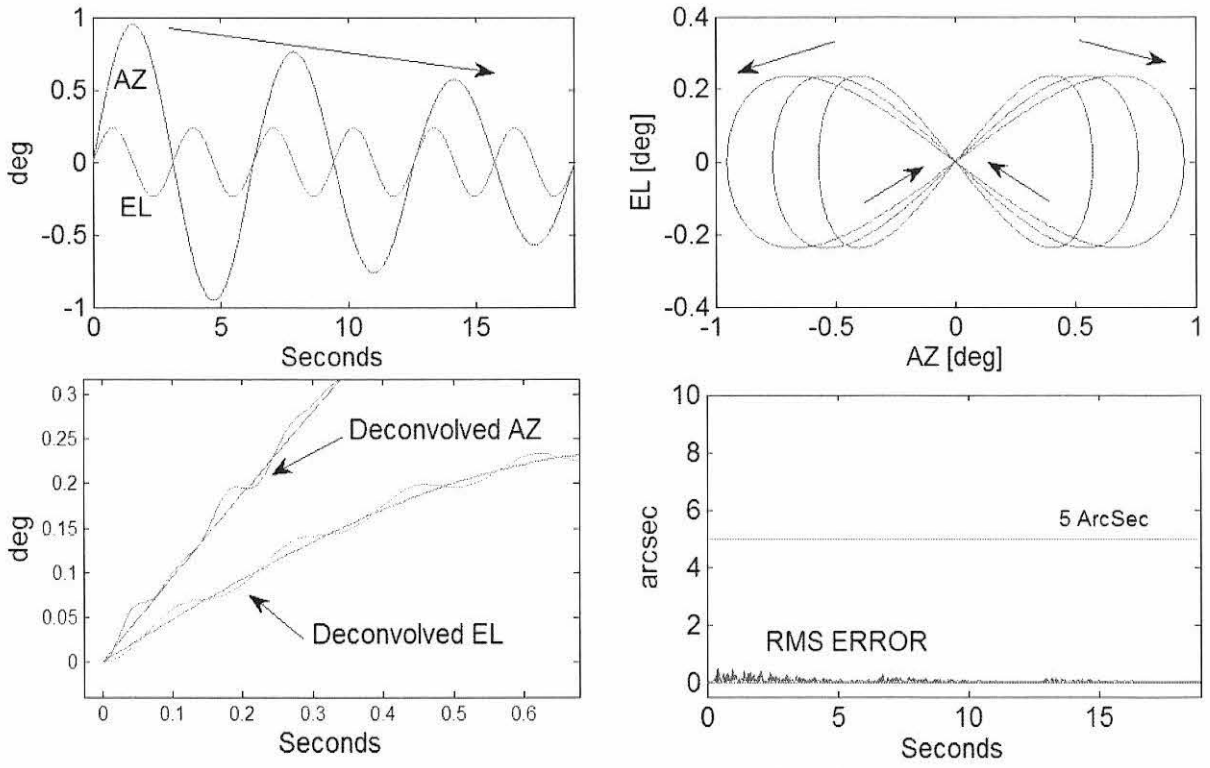

Figure 11: De-convolution example for a 1000 micron Lissajous scan

The scan pattern is a sinusoid in each axis with a decreasing gain in the AZ-axis. The single-axis and combined-axis time responses are shown in the top parts of Figure 11. The covered region on-the-sky is a rectangle with rounded corners. The pattern in this example is not meant to be used during observations but it is of sufficient complexity to demonstrate the method. The input lasts for 20 seconds, and the entire 20 second input and output are used to estimate 20 seconds of the impulse response. The first pass of the input is a test pattern used to determine the distorted input, and then a second pass is used to collect scientific data. A small portion of the input and the distorted input are shown in the lower left of the figure. The achieved rms error is shown in the lower right part of the figure and is well below the half-beamwidth error bound of 5 ArcSec. Furthermore, the error criterion is immediately satisfied without having to wait for settling.

7. CONCLUSIONS

A preliminary design of the CCAT mount control system is presented. The mount control design is based on a finite element model of the structure. The feedback signals are velocity and position signals, both derived from an encoder. Torque commands are computed using a PID compensator and a structural filter. Command response is improved using feedforward and command shaping. These parts of the mount control system can be described as "classical" or "conventional." Less conventional, innovative parts of the controller are the two command path command shaper, which is needed to meet fast nodding requirements, and the de-convolution method for commanding fast scans.

The wind jitter requirement of 0.2 ArcSec is not satisfied by 50 percent or more, depending on the wind model. Changes to the structure are being considered. Changes to the control system to include additional sensors are also being considered. The additional sensors are accelerometers and wind pressure sensors.

CCAT will implement fast scans using Lissajous patterns. Reasons why this is a challenge for conventional mount control are presented. The proposed method uses de-convolution to pre-distort input signals, where the de-convolution is based on an estimate of the closed loop impulse response. The required accuracy is very high, less than and possibly much less than one percent. The example presented here uses the scan as a test signal, thereby requiring two passes for a given scan. Probably a shorter test signal can be used, which is one of the issues that will be studied going forward. Other issues going forward are how often the impulse response estimate needs to be updated, how sensitive the impulse response estimate is to wind disturbance, and whether or not additional pre-distortion is needed to account for the flexible structure.

REFERENCES

[1] CCAT project website: http://www.ccatobservatory.org
[2] Kan, Frank, "Finite Element Model of CCAT," Contractor Report, Feb. 2013.
[3] Thompson, Peter M. and Steve Padin, "CCAT Mount Control Design," STI-TR-2703-01, Sept. 2013.
[4] Padin, Steve, "Drive Architecture Technical Requirements," CCAT-TR-21, Sept. 2012.
[5] Padin, Steve, "CCAT Drive," CCAT-TM-96, June 2012.
[6] Thompson, Peter M., Douglas G. MacMynowsky, and Mark J. Sirota, "Analysis of TMT Mount Control System," SPIE, 2008.
[7] Thompson, Peter M., Tomas Krasuski, Kevin Tsubota, and Jimmy Johnson, "Keck telescope mount control redesign to improve short move performance," SPIE, 2014.
[8] Conversation with Doug MacMartin, 2013.